  Bull. Chem. Soc. Jpn., 56, 3393—3399 (1983)

Amorphous Ni–Ti and Ni–Zr Alloys for Water Electrolysis Cathode Materials

Ken-ichi MACHIDA, Michio ENYO,* Isamu TOYOSHIMA, Koshiro MIYAHARA, Kenzo KAI,† and Kenji SUZUKI†

Research Institute for Catalysis, Hokkaido University, Sapporo 060

†*The Research Institute for Iron, Steel, and Other Metals, Tohoku University, Sendai 980*

(Received May 13, 1983)

Amorphous Ni–Ti and Ni–Zr alloys for their possible use in water electrolysis cathode materials were investigated. The hydrogen electrode reaction in 1 M NaOH (1 M = 1 mol dm^{-3}) proceeds *via* the Volmer-Tafel reaction route with mixed rate-determining characteristics. The electrocatalytic activity is augmented significantly with a treatment of the alloy electrodes with aq HF. Thus, the exchange current density reaches 10^{-3} A cm^{-2} (apparent) at 303 K. The activation energy values are 9.4, 5.5, and 6.1 kcal mol^{-1} (1 cal = 4.184 J) for the Volmer and Tafel step and the overall reaction, respectively. Surface analyses of the electrodes have indicated that such a high activity is caused by a stable porous Ni layer which is formed on the surface by the acid treatment. Such a porous Ni layer was not effectively formed if the alloys were in crystalline states.

Hydrogen is noted as a possible candidate for an energy carrier in the future as it is clean and fully recycleable substance of practically unlimited supply.[1] The energy system with hydrogen would consist mainly of three processes, the generation, transport or storage, and utilization. For its generation, the electrolysis of water is a simple and well established technique but, to make the technique economically practicable, improvements in electrode materials towards a minimized energy consumption are required.

Most of amorphous alloys prepared by a rapid quench from their melts, in general, possess high mechanical and corrosion resistant properties, and hence some of them have already been investigated for catalyst or electrode materials uses.[2,3] Also, a number of amorphous alloys, such as Ni alloys, containing, Ti, Zr, or Th, have been investigated towards hydrogen storage materials since they are not pulverized upon absorption and liberation of hydrogen and, in addition, have an improved amount and rate of absorption of hydrogen as compared with the corresponding crystalline alloys.[4] This indicates that there might be a possibility of using the amorphous alloys not only for a hydrogen evolving cathode but also for a hydrogen storage electrode.

One of the present authors investigated ealier the kinetics and mechanism of the hydrogen electrode reaction on Pd, a typical hydrogen absorbing metal.[5] It has been shown that the component overpotentials for each of the constituent steps are individually observable owing to the existence of a large amount of hydrogen stored in the electrode metal. Analysis of the overpotential rise and decay transient curves has shown that the hydrogen electrode reaction on Pd is comprised of two elementary steps, namely, Volmer and Tafel processes. The reaction rates of the elementary steps have thence been evaluated.

In this paper, we report the hydrogen electrode reaction characteristics of amorphous Ni–Ti and Ni–Zr alloys. In particular, the relationship between the electrodic property and the surface state of these electrodes will be discussed.

Experimental

Preparation of Electrodes. The amorphous alloys were prepared from the melts by a rapid quenching using a single roller type apparatus.[6] The specimens are of the following compositions, $Ni_{0.27}Ti_{0.73}$, $Ni_{0.33}Ti_{0.67}$, $Ni_{0.40}Ti_{0.60}$, $Ni_{0.25}Zr_{0.75}$, $Ni_{0.33}Zr_{0.67}$, $Ni_{0.50}Zr_{0.50}$, and $Ni_{0.65}Zr_{0.35}$. The crystalline Ni–Ti and Ni–Zr alloys were obtained by annealing the amorphous alloys at 873—1073 K for 30 min under a He atomosphere (20—30 kPa). The phase transition from the amorphous to the crystalline phase was monitored by observing changes of the electric conductivity and detected later by an X-ray diffraction analysis.

The specimens were in the shape of a ribbon, 0.6—1.4 mm in width, *ca.* 20 μm in thickness, and 1—2 cm in length, with the apparent surface area of 0.05—0.15 cm^2. Their ends were spot-welded to nickel wire which was in turn sealed into 8 mmϕ Pyrex glass tubings with epoxy resin ("Torr Seal" Varian Associates). These electrodes were treated with hot concentrated H_2SO_4, aqua regia, or 1 M HF solution in order to remove the oxide film on the surface (see below).

Electrochemical Measurements. The electrochemical measurements were carried out in a three compartment Pyrex glass electrolysis cell under a stream of H_2. A platinized Pt electrode was also used for comparison. The electrolytic solution, 1 M NaOH, was prepared from special grade NaOH (Merck Japan, Ltd.) with water from a Millipore pure water system. The temperature was controlled by a thermostat at 303 K except for the temperature dependence experiments. Details of the method and apparatus of the electrochemical measurements were described in a previous paper.[7]

X-Ray Photoelectron Spectroscopy. The surface analysis was performed by employing an ESCA apparatus (VG-III). Ar^+ bombardments were carried out at a condition of 800 eV and 3 μA cm^{-2} for 20 min in order to remove adsorbed carbon or hydroxyl groups from the surface of the alloys and to enhance the sensitivity of the detection. The spectra obtained were calibrated with the $4f_{7/2}$ peak from an Au plate which was employed as an internal standard. In order to avoid the overlap of the main spectra of Ti or Zr and Ni with their Auger signals, Al $K\alpha$ and Mg $K\alpha$ radiations were used for the Ni–Ti and Ni–Zr alloys, respectively.

Results and Discussion

Electrochemical Properties. The electrocatalytic activity of the amorphous Ni–Ti and Ni–Zr alloy electrodes in as-obtained form or after treatments with hot concentrated H_2SO_4 or aqua regia were very low and the reversible hydrogen electrode potential was not observed. However, when the samples, both the amorphous and crystalline alloys, were etched with a HF solution (1 M) for several minutes, the activity was strongly enhanced and the reversible potential was established. Alloys with relatively high Ni contents tended to require longer periods of time of the HF-treatment for the activation.

The galvanostatic overpotential rise transients give the rapidly growing overpotential component, η_1, which has the characteristics attributable to the Volmer process.[5,8] In Fig. 1 are shown the cathodic and anodic polarization behaviors with respect to η_1 on a series of the amorphous Ni–Ti alloys. The cathodic and anodic polarization curves appear to be essentially symmetrical with each other about the abscissa. This is expressed in terms of the symmetry factor β, which can be evaluated if we calculate the cathodic unidirectional current i_{-v}, by the relation,[5,8] $i_{-v}=i_{ov}\exp[-\beta F\eta/RT]=i/[1-\exp(F\eta/RT)]$. This is also shown in Fig. 1, a dashed line ($Ni_{0.27}Ti_{0.73}$), which gives almost a straight line with the slope of ≈ 95 mV or $\beta\simeq 0.63$. It is, therefore, concluded that η_1 represents the overpotential component responsible for an one electron transfer reaction, namely the Volmer (discharge) step.

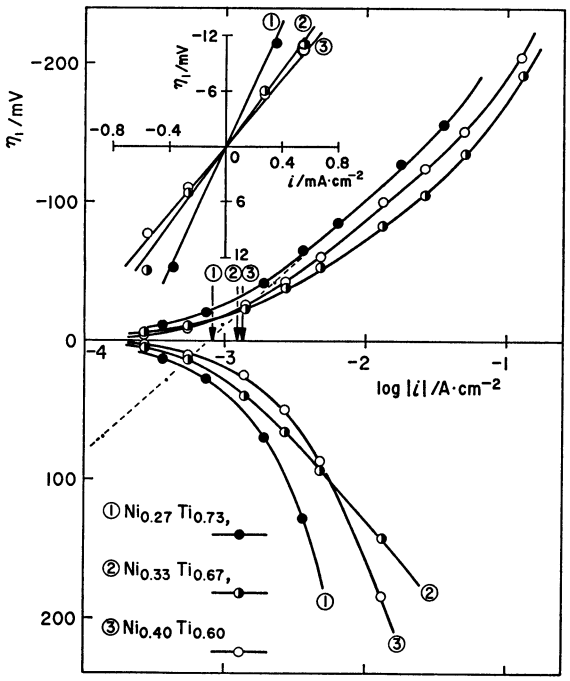

Fig. 1. Cathodic and anodic polarization behaviors of the rapidly rising overpotential component η_1 on a series of amorphous Ni–Ti alloys. The arrows on the abscissa indicate i_{ov} as evaluated from the linear plots (the inset figure) of η_1 *vs.* i near the reversible hydrogen electrode potential. 1 M NaOH, 303 K.

The exchange current density i_{ov} of the Volmer step has been evaluated[8] from the slope of a linear plot

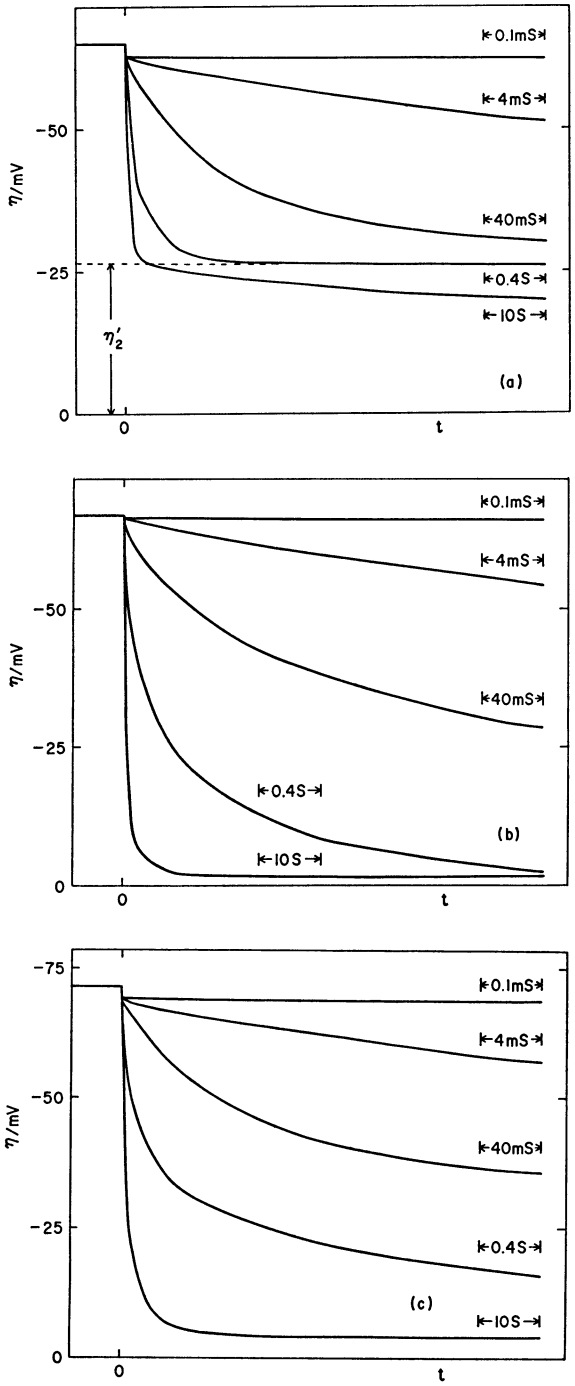

Fig. 2. Overpotential decay transients with various time scales. 1 M NaOH, 303 K.
(a) Amorphous $Ni_{0.33}Ti_{0.67}$ alloy electrode after a treatment with 1 M HF solution. $i=2.40$ mA cm^{-2} (apparent). (b) Crystalline $Ni_{0.33}Ti_{0.67}$ alloy electrode after a treatment with 1 M HF solution. $i=0.27$ mA cm^{-2} (apparent). (c) Amorphous $Ni_{0.33}Zr_{0.67}$ alloy electrode after a treatment with 1 M HF solution. $i=1.91$ mA cm^{-2} (apparent).

†† The current density and the exchange current densities are given, unless otherwise stated, on the apparent unit area basis.

of η_1 *vs.* current density at low overpotentials (the polarization resistance, r_1) with $i_{oV}=(RT/F)/r_1$. On the amorphous Ni–Ti alloy electrodes, i_{oV} was found to be of the order†† of 10^{-3} A cm^{-2} and did not depend appreciably on the alloy composition. The values are indicated by the arrows on the abscissa in Fig. 1.

The overpotential decay transients at various time scales on the amorphous and crystalline $Ni_{0.33}Ti_{0.67}$ alloy electrodes are shown in Figs. 2(a) and 2(b), respectively. The overpotential on the amorphous electrode decayed rapidly up to about 1 sec but, after that, the decay rate was greatly diminished so as to require several minutes for its complete decay (Fig. 2(a)). On the crystalline alloy electrodes, on the other hand, the overpotential decayed much more rapidly and no plateau was observed on the transient curves (Fig. 2(b)). These observations suggest that the rate of hydrogen absorption into or liberation from the amorphous Ni–Ti alloys is very rapid as compared with the surface reaction, but that may not be the case with the crystalline alloys.

The slowly decaying overpotential component η_2' is defined at the moment of completion of the initial rapid overpotential decay upon the termination of the polarization current. This was readily evaluated on the amorphous Ni–Ti electrodes by extrapolating the plateau on the overpotential decay curves, such as that in Fig. 2(a), to $t=0$. Results are shown in Fig. 3, together with the total overpotential η on the amorphous or cyrstalline Ni–Ti alloys, and also η on a platinized Pt electrode. The slope of the Tafel lines for η_2' was around 30 mV and the exchange current density value, evaluated by $i_{oT}=(RT/2F)/r_2'$ where r_2' is the polarization resistance with respect to η_2', was around 0.4×10^{-3} A cm^{-2}. The fact that the latter value is not much different from i_{oV} reported above indicates that the hydrogen electrode reaction is of mixed rate-determining type.

The Tafel slope and the exchange current density values associated with η_2' suggest, along with the Tafel (H(a) recombination) step, a significant contribution to η_2' of the H_2 diffusion process in the solution phase. To see this, the diffusion overpotential in the present experimental system was evaluated separately using a Au electrode of a similar dimension. As the overpotential on Au decays very rapidly (time constant $\approx10^{-3}$ s) except for a component attributed to the concentration overpotential due to H_2 diffusion, the overpotential decay transients could reveal only the latter component (the time constant $\approx10^{0}$ s). Results indicated that the concentration overpotential is of comparable magnitude with η_2'. This means that i_{oT} as determined from η_2' is in fact for the Tafel-plus-diffusion processes and hence the intrinsic value for the Tafel step should be considerably greater than the value quoted above or given below in Table 1.

The linear portion of the Tafel line with respect to the total overpotential η in the cathodic region has the slope of about 120 mV and its extrapolation to $\eta=0$ gives the exchange current density $i_{o,ext}$ of the order of 10^{-3} A cm^{-2}. It has been shown earlier from a general analysis of the mixed rate-determining Volmer-Tafel reaction[8] that the kinetics at high cathodic overpotentials should practically be determined by the Volmer step. This means that the electrocatalytic activity of the electrode under (deep) cathodic polarization is approximately represented by i_{oV} and not i_o or i_{oT}. Indeed, comparison of Fig. 3 with Fig. 1 reveals that $i_{o,ext}$ is in fair agreement with i_{oV} reported above.

In Table 1 are summarized the exchange current densities and the double layer capacitance obtained on the amorphous or crystalline Ni–Ti alloys, a Ni wire (0.25 mmϕ), and a platinized Pt electrode.

The exchange current density i_o of the overall reaction on the amorphous Ni–Ti electrodes is calculated from i_{oV} and i_{oT} by the relation,

$$\frac{1}{i_o}=\frac{1}{i_{oV}}+\frac{1}{i_{oT}}.$$

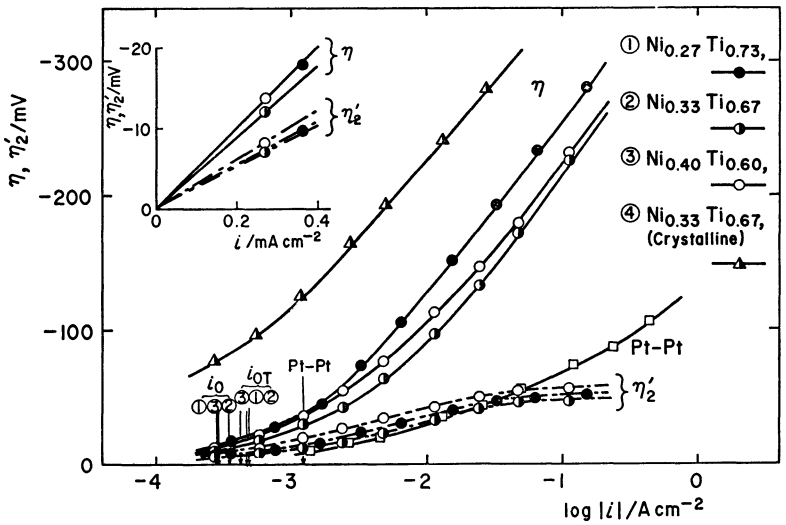

Fig. 3. Cathodic polarization behaviors of the total overpotential η and slowly decaying overpotential component η_2' on a series of amorphous and crystalline Ni–Ti alloy electrodes and on platinized Pt electrode. The arrows on the abscissa indicate i_o and i_{oT} obtained at low overpotentials (the inset figure). 1 M NaOH, 303 K.

Table 1. Exchange current densities[a] of the elementary steps and the overall reaction and the double layer capacitance on the cathodes of a series of Ni-Ti alloys in 1 M NaOH at 303 K

Composition	State	i_{oV} / mA cm^{-2}	i_{oT} / mA cm^{-2}	i_o / mA cm^{-2}	$i_{o,ext}$ / mA cm^{-2}	C / mF cm^{-2}
$Ni_{0.27}Ti_{0.73}$	Amorphous	0.82	0.47	0.28	0.83	2.3
$Ni_{0.33}Ti_{0.67}$	Amorphous	1.22	0.49	0.35	1.80	4.7
$Ni_{0.40}Ti_{0.60}$	Amorphous	1.32	0.37	0.29	1.60	2.1
$Ni_{0.33}Ti_{0.67}$	Crystalline				0.10	0.4
Ni	Crystalline				0.006	0.1
Pt-Pt	Crystalline			1.22		40.2

a) Per apparent unit area.

As mentioned above, i_o should not be identified with $i_{o,ext}$ in mixed rate-determining reactions such as in the present case ($i_o < i_{o,ext} \simeq i_{oV}$).

The evaluation of the step rates from the component overpotentials was not possible on the crystalline Ni–Ti electrode or on the Ni wire electrode. Accordingly, only $i_{o,ext}$ values are given, which may be compared with i_{oV}, at least approximately, as discussed above.

It is seen in Table 1 that the amorphous Ni–Ti alloy electrodes have electrocatalytic activities higher than the crystalline alloy electrode and far greater than that of the pure Ni electrode. The rate can further be increased if the H_2 diffusion rate were raised by improved stirring, *etc.* Even in the present stage, the activity is almost comparable with that of a smooth Pt electrode, particularly at low current densities.

It was seen that such a high electrocatalytic activity on the amorphous alloy electrodes were caused by a very large roughness factor value that was realized. The factor is evaluated from the capacitance values in Table 1 to be several hundreds, if one assumes a value of 18 μF cm^{-2} usually observed on Hg electrode to be the value per true unit area. Such an increase of the surface roughness factor must be a result of dissolution of the component metal Ti in the alloys by the treatment with hydrofluoric acid. If one counts $i_{o,ext}$ per true unit area on the amorphous and crystalline alloys, they are always in the range of 10^{-6}—10^{-5} A cm^{-2} (true) and are very close to that generally observed on smooth Ni electrodes. This is an indication that the electrocatalytic activity is caused by the layer of Ni and not by Ti.

The heat of activation determined from the Arrhenius plots of the exchange current densities (Fig. 4) on the amorphous $Ni_{0.33}Ti_{0.67}$ electrode was about 9.4, 5.5, and 6.1 kcal mol^{-1} for the Volmer and Tafel/diffusion step and the overall reaction, respectively. The value for the Volmer process was well comparable with the corresponding value of 8 kcal mol^{-1} observed on Pd.[8] The value for the Tafel/diffusion process is larger than *ca.* 3 kcal mol^{-1} anticipated for the diffusion process itself and thus indicates a significant contribution from the Tafel step which is likely[8] to be associated with some 6 kcal mol^{-1}.

The overpotential decay transients on the amorphous Ni–Zr alloy ($Ni_{0.33}Zr_{0.67}$) are shown in Fig. 2(c). The overpotential on both the amorphous and

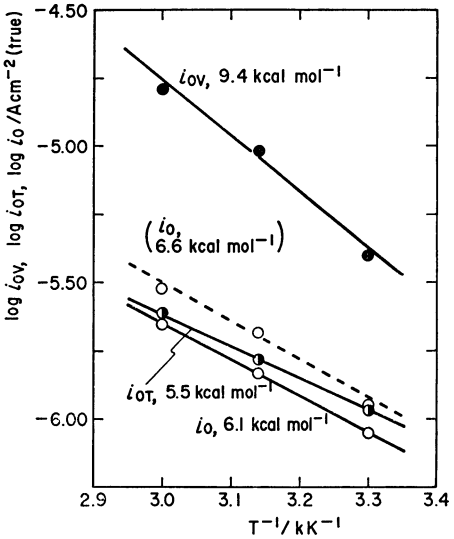

Fig. 4. Arrhenius plots of the exchange current densities and corresponding activation heats of the Volmer and Tafel step and the overall reaction on the amorphous $Ni_{0.33}Ti_{0.67}$ alloy electrode. The dashed-line and the value in the parenthesis represent those of i_o on the amorphous $Ni_{0.33}Zr_{0.67}$ alloy electrode. 1 M NaOH.

crystalline Ni–Zr alloys decayed rapidly with no plateau, and hence the kinetics of the component elementary reactions were not obtainable. Likewise, the evaluation of η_1 from the galvanostatic overpotential rise transients were not practicable.

The overall polarization characteristics on the amorphous or crystalline Ni–Zr alloys are shown in Fig. 5. It is seen that the electrodic characteristics are very similar with those of the Ni–Ti alloys. Thus, the slope of the Tafel line is around 120 mV and $i_{o,ext}$ is around 10^{-3} A cm^{-2}. One may hence conclude that the hydrogen electrode reaction on these alloys also proceeds *via* the Volmer-Tafel route with practically the same electrocatalytic activities, respectively, with the amorphous or crystalline Ni–Ti alloys reported above.

The polarization resistance around the reversible potential gives the values of i_o which are roughly in one order of magnitude smaller than $i_{o,ext}$. Along the line of arguments presented above, this fact may indicate that i_{oT} is at least several times smaller than

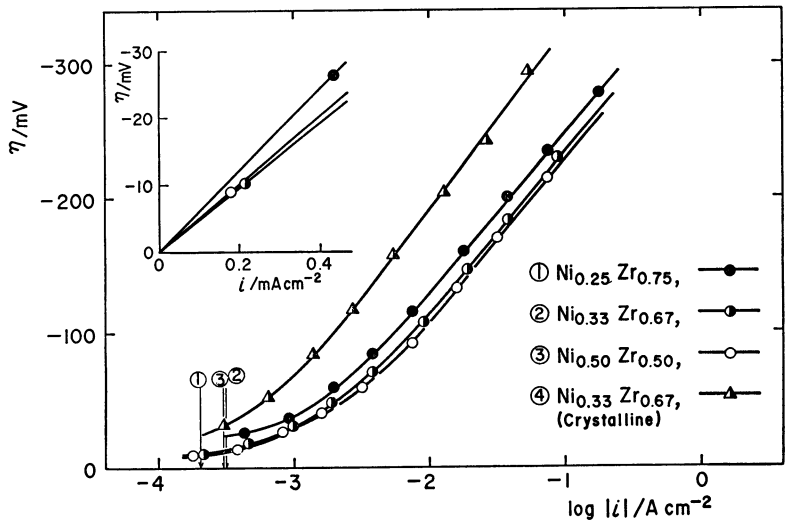

Fig. 5. Cathodic polarization behaviors of the total overpotential η on a series of the amorphous and crystalline Ni–Zr alloy electrodes. The arrows on the abscissa indicate i_o obtained at low overpotentials (the inset figure). 1 M NaOH, 303 K.

Table 2. Exchange current densities[a] and double layer capacitance on the cathodes of a series of Ni–Zr alloys in 1 M NaOH at 303 K

Composition	State	i_o / mA cm^{-2}	$i_{o,ext}$ / mA cm^{-2}	C / mF cm^{-2}
$Ni_{0.25}Zr_{0.75}$	Amorphous	≈0.2	0.81	5.0
$Ni_{0.33}Zr_{0.67}$	Amorphous	≈0.3	1.10	4.1
$Ni_{0.50}Zr_{0.50}$	Amorphous	≈0.3	1.30	2.8
$Ni_{0.33}Zr_{0.67}$	Crystalline		0.34	0.9

a) Per apparent unit area.

i_{oV} and hence $i_o \simeq i_{oT}$. Values of i_o are hence evaluated by $i_o=(RT/2F)/r$ with $r=(d\eta/di)_{\eta\to o}$ in a similar manner as i_{oT}. These are indicated by arrows in Fig. 5.

The exchange current density and the double layer capacitance obtained on a series of the amorphous Ni–Zr alloys and the crystalline $Ni_{0.33}Zr_{0.67}$ alloy are given in Table 2. Electrocatalytic activity measurements on $Ni_{0.65}Zr_{0.35}$ were unsuccessful because of its very low activity. The values of i_o on the amorphous Ni–Zr alloys was 0.2—0.3 mA cm^{-2}. As seen from Fig. 5, the electrocatalytic activity of the amorphous Ni–Zr alloys is considerably higher than that of the crystalline ones as in the case of the Ni–Ti systems. Also, it can be seen from Table 2 that the amorphous Ni–Zr alloys give nearly the same values of the double layer capacitance as on the amorphous Ni–Ti alloys and hence their true surface area is also very large.

The heat of activation was determined only for the overall reaction. It was 6.6 kcal mol^{-1} on the $Ni_{0.33}Zr_{0.67}$ alloy, as already shown in Fig. 4.

Surface Characterization. Surface analysis of the Ni–Ti or Ni–Zr alloy electrodes before and after the treatment with hydrofluoric acid were performed using the X-ray photoelectron spectroscopy (XPS) method. In Fig. 6 are recorded typical XPS spectrum patterns on the amorphous $Ni_{0.33}Ti_{0.67}$ and $Ni_{0.33}Zr_{0.67}$ alloys over a wide range of the binding energy. The nontreated (as-obtained) alloys, spectra a) ($Ni_{0.33}Ti_{0.67}$) and c) ($Ni_{0.33}Zr_{0.67}$), gave the signals with strong intensity of Ti or Zr and O, whereas the peaks to be assigned to Ni were very weak and almost undetectable. On the other hand, on the HF-treated samples, the

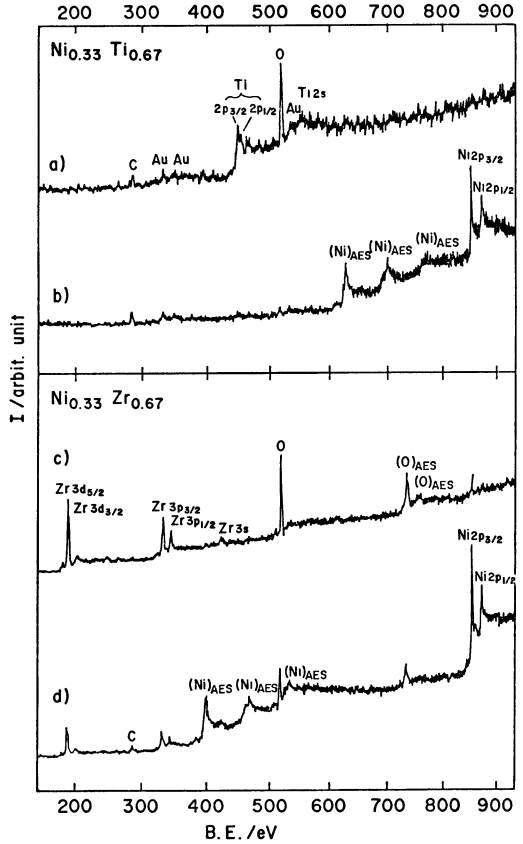

Fig. 6. XPS spectrum patters of the amorphous $Ni_{0.33}Ti_{0.67}$ and $Ni_{0.33}Zr_{0.67}$ alloys obtained with a wide range scan of the binding energy (*B.E.*=0—1000 eV). The X-ray source employed was Al $K\alpha$ for $Ni_{0.33}Ti_{0.67}$ and Mg $K\alpha$ for $Ni_{0.33}Zr_{0.67}$, respectively. a) and c), nontreated specimens; b) and d), HF-treated specimens.

XPS and Auger electron spectra from Ni increased remarkably while the signals of Ti or Zr were diminished (spectra b) and d)).

Figure 7 shows the XPS spectra ascribed to the Ti_{2p} or Zr_{3d} and the O_{1s} electrons from the nontreated amorphous $Ni_{0.33}Ti_{0.67}$ and $Ni_{0.33}Zr_{0.67}$ alloys. The signals of $Ti_{2p3/2}$ (or $Ti_{2p1/2}$) consists of three bands, as deconvoluted in Fig. 7, with the peak values around 455, 457, and 459 eV (or 461, 463, and 464.5 eV). These are attributable to metallic Ti or two oxides, Ti_2O_3 and TiO_2, on the basis of the data given in a handbook.[9] The Ti_2O_3 was probably formed from TiO_2 by the Ar^+ bombardments.[10] The $Ti_{2p3/2}$ and $Ti_{2p1/2}$ signals gave energy differences of 6.1 eV for metallic Ti or Ti_2O_3 and 5.6 eV for TiO_2. These values are in good agreement with the values in the literatures[9,11] for titanium in such valence states.

For the $Zr_{3d5/2}$ and $Zr_{3d3/2}$ electrons, there are each two bands respectively assigned to the Zr metal and its oxide (ZrO_2), with the peak positions about 179 or 182 eV for the former zirconium and about 183 or 185 eV for the latter one. The energy gaps of $Zr_{3d5/2}$ and $Zr_{3d3/2}$ were 2.3—2.4 eV as expected.[9] The O_{1s} signals are attributable to the lattice oxygens of Ti_2O_3, TiO_2, or ZrO_2. The XPS profiles similar to the Ti_{2p}, Zr_{3d}, or O_{1s} spectra in Fig. 7 were observed on the other amorphous or crystalline alloys.

The findings indicate that most of Ti or Zr on the surface of the alloys exists as dioxide, *viz.* TiO_2 or ZrO_2. On the other hand, the peak positions of $Ni_{2p3/2}$ and $Ni_{2p1/2}$ (≈853 and 870 eV) and the energy differences between these signals (≈17 eV) indicate that the nickel on the surface is metallic.

The surface atomic ratios, $C^S_{Ni/Ti}$ and $C^S_{Ni/Zr}$, were calculated from the integral peak intensity (I) of Ni_{2p} and $Ti_{2p3/2}$ or $Zr_{3d5/2}$, after taking into account their atomic sensitivity factors (S)[9] for X-ray in the following equation:

$$C^S_{Ni/M} = (I_{Ni}/S_{Ni})/(I_M/S_M), \quad M = Ti, Zr,$$

where the values employed were $S_{Ni}=5.4$, $S_{Ti}=1.1$, and $S_{Zr}=0.87$. The relationship between the surface and bulk Ni/Ti and Ni/Zr atomic ratios is shown in Fig. 8. It is seen that $C^S_{Ni/Ti}$ or $C^S_{Ni/Zr}$ values on the nontreated (amorphous and crystalline) samples are very low and entirely different from their bulk compositions. Thus, electrode surface is almost completely covered with a film of TiO_2 or ZrO_2. This explains why their electrocatalytic activity in the original form was so low that the reversible hydrogen electrode potential was hardly realized.

On the HF-treated alloys, the ratios $C^S_{Ni/Ti}$ and $C^S_{Ni/Zr}$ were found to be much higher than the values of $C^B_{Ni/Ti}$ and $C^B_{Ni/Zr}$ and this was particularly true on the amorphous alloys. It is conceivable that the concentration of Ni on the alloys would be increased by this treatment, above the level of its bulk composition, as hydrofluoric acid readily attacks the metal or oxides of Ti or Zr but not Ni. Further, the sufrace of the HF-treated alloys is very porous with the roughness factor as high as 300, as evaluated above from the

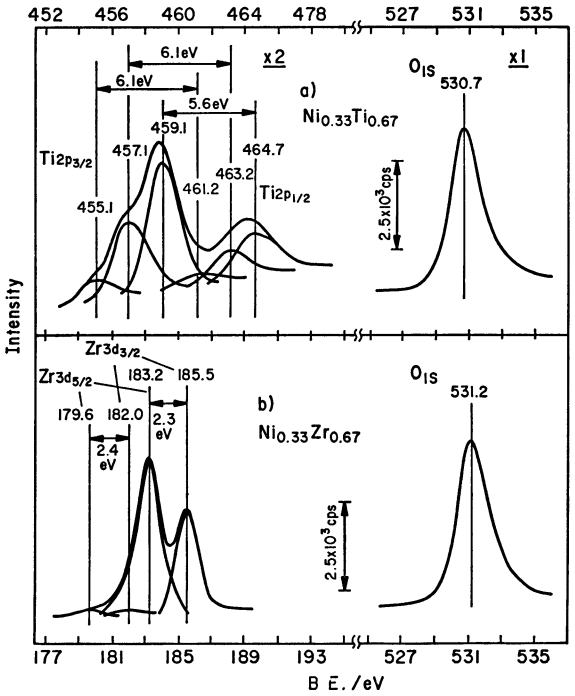

Fig. 7. XPS spectra of the Ti_{2p} or Zr_{3d} and the O_{1s} electrons from the amorphous $Ni_{0.33}Ti_{0.67}$ and $Ni_{0.33}Zr_{0.67}$ alloys (nontreated specimens). The X-ray source employed was Al $K\alpha$ for $Ni_{0.33}Ti_{0.67}$ and Mg $K\alpha$ for $Ni_{0.33}Zr_{0.67}$, respectively. The spectra of Ti_{2p} and Zr_{3d} were deconvoluted using Gaussian curves with reasonable half-band widths.

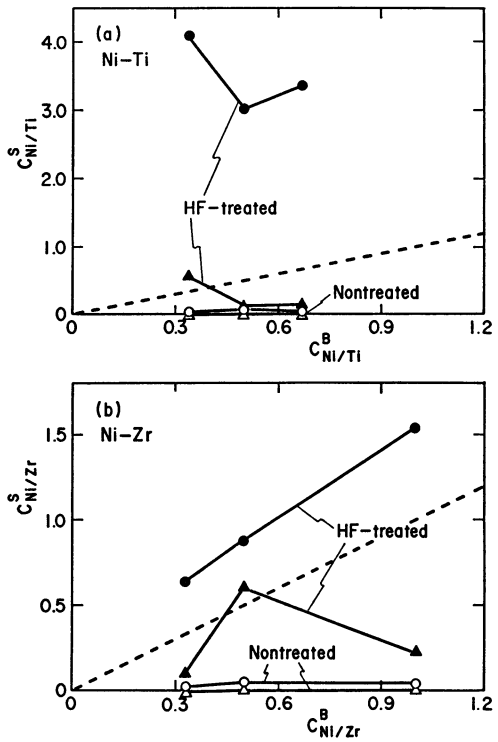

Fig. 8. Relationship between the surface and bulk atomic ratios ($C^S_{Ni/M}$ and $C^B_{Ni/M}$, M=Ti, Zr) of (a) Ni-Ti and (b) Ni-Zr alloys before and after the acid treatments. The dashed line represents a linear relationship of $C^S_{Ni/M}$ and $C^B_{Ni/M}$ when the surface concentration of the alloys is equal to the bulk one. Amorphous, ○ and ●; Crystalline, △ and ▲.

double layer capacitance (see Tables 1 and 2).††† The high electrocatalytic activity observed above is probably caused by the Ni-rich surface layer which is in the form of a Raney-type nickel. Indeed, the electrocatalytic activities per true unit area of the amorphous or cyrstalline Ni–Ti and Ni–Zr alloy electrodes are of the same order of magnitude with those on pure nickel electrodes.

It may be stressed that the amorphous, but not the crystalline, alloys could be readily brought to the state of very high roughness factor and hence of very high electrocatalytic activity by a simple acid treatment.

Conclusion

The amorphous Ni–Ti and Ni–Zr alloys after the treatment with aqueous HF have high electrocatalytic activity for the hydrogen electrode reaction in alkaline solutions. This is caused firstly by the removal of an inert film of TiO_2 of ZrO_2 from the surface, and secondly by producing a porous layer of Ni, which is stable on the amorphous alloys. Since the amorphous alloys in general show a high mechanical strength and high corrosion resistance, they can possibly be employed as water electrolysis cathode materials for hydrogen generation by water electrolysis.

††† The fact that the amorphous $Ni_{0.65}Zr_{0.35}$ alloy do not give an active electrode is likely to be due to a difficulty of removing Zr from the matrix by the acid treatments because of the high Ni content.

The present work is supported in part by Grants-in-Aid for Scientific Research No. 56119004 from the Ministry of Education, Science and Culture. Supports from the Mitsubishi Foundation, 1979, and from Ohtsuka Chemicals Co. Ltd. are also gratefully acknowledged.

References

1) G. G. Libowitz, "Hydrides for Energy Storage," ed by A. F. Andresen and A. J. Maeland, Pergamon Press, New York (1978), pp. 1—17.
2) A. Yokoyama, H. Komiyama, H. Inoue, T. Masumoto, and H. Kimura, *Shokubai*, **24**, 61 (1982).
3) a) M. Hara, K. Asami, K. Hashimoto, and T. Masumoto, *Electrochim. Acta*, **25**, 1091 (1980); b) K. Hashimoto and M. Hara, *Denki Kagaku*, **49**, 446 (1981).
4) a) A. J. Maeland, L. E. Tanner, and G. G. Libowitz, *J. Less-Common Met.*, **74**, 279 (1980); b) K. Aoki, A. Horata, and T. Masumoto, *Sci. Rep. Res. Inst. Tohoku Univ.*, **A29**, 218 (1981).
5) M. Enyo and T. Maoka, *J. Electroanal. Chem.*, **108**, 277 (1980).
6) M. Matsuura, M. Kikuchi, M. Yagi, and K. Suzuki, *Jpn. J. Appl. Phys.*, **19**, 1781 (1980).
7) T. Maoka and M. Enyo, *Surf. Technol.*, **8**, 441 (1979).
8) M. Enyo, *J. Electroanal. Chem.*, **134**, 75 (1982).
9) C. D. Wagner, W. M. Riggs, L. E. Davis, J. F. Moulder, and G. E. Muilenberg, "Handbook of X-Ray Phoelectron Spectroscopy," Perkin-Elmer Co., Physical Electronics Div. (1979).
10) B. A. Sexton, A. E. Hughes, and K. Foger, *J. Catal.*, **77**, 85 (1982).
11) T. L. Barr, *J. Phys. Chem.*, **82**, 1801 (1978).